antibodies used were Mouse anti-Glial Fibrillary Acidic Protein (GFAP) (1:200; MAB360; Chemicon, Millipore, MA, USA), mouse anti-C38 (1:200; provided by Dr. Jun Kosaka), rabbit anti-NCK2 (1:200; ab14590; Abcam), or rabbit anti-HK2 (1:200; 2867S; Cell Signaling Technology, MA, USA). The sections were washed three times with PBST (PBS containing 0.2% Tween 20) and then incubated with secondary goat anti-rabbit IgG antibody (1:200; A11008 Invitrogen, Carlsbad, CA, USA) tagged with Alexa 488 or goat anti-mouse IgG A11030; Invitrogen, Carlsbad, CA, USA) tagged with Alexa 546 for 1 hour. The slides were washed three times and mounted with Vectashield mounting medium (H1000; Vector, Burlingame, CA).

References

1. Quigley H (1996) Number of people with glaucoma worldwide. Br J Ophthalmol 80: 389–393.
2. Quigley H (1993) Open-angle glaucoma. N Engl J Med 328: 1097–1106.
3. Hitchings RA, Anderton SA (1983) A comparative study of visual field defects seen in patients with low-tension glaucoma and chronic simple glaucoma. Br J Ophthalmol 67: 818–821.
4. Hitchings R (1992) Low tension glaucoma–its place in modern glaucoma practice. Br J Ophthalmol 76: 494–496.
5. Werner E (1996) Normal-tension glaucoma.; Ritch R SM, Krupin T, eds., editor. St.Louis: Mosby. 769–797 p.
6. Shiose Y, Kitazawa Y, Tsukahara S, Akamatsu T, Mizokami K, et al. (1991) Epidemiology of glaucoma in Japan–a nationwide glaucoma survey. Jpn J Ophthalmol 35: 133–155.
7. Iwase A, Suzuki Y, Araie M, Yamamoto T, Abe H, et al. (2004) The prevalence of primary open-angle glaucoma in Japanese: the Tajimi Study. Ophthalmology 111: 1641–1648.
8. Raymond V (1997) Molecular genetics of the glaucomas: mapping of the first five "GLC" loci. Am J Hum Genet 60: 272–277.
9. Sarfarazi M (1997) Recent advances in molecular genetics of glaucomas. Hum Mol Genet 6: 1667–1677.
10. Liu Y, Allingham RR (2011) Molecular genetics in glaucoma. Exp Eye Res 93: 331–339.
11. Pasutto F, Keller KE, Weisschuh N, Sticht H, Samples JR, et al. (2012) Variants in ASB10 are associated with open-angle glaucoma. Hum Mol Genet 21: 1336–1349.
12. Burdon KP, Macgregor S, Hewitt AW, Sharma S, Chidlow G, et al. (2011) Genome-wide association study identifies susceptibility loci for open angle glaucoma at TMCO1 and CDKN2B-AS1. Nat Genet 43: 574–578.
13. Ramdas WD, van Koolwijk LM, Lemij HG, Pasutto F, Cree AJ, et al. (2011) Common genetic variants associated with open-angle glaucoma. Hum Mol Genet 20: 2464–2471.
14. Wiggs JL, Yaspan BL, Hauser MA, Kang JH, Allingham RR, et al. (2012) Common variants at 9p21 and 8q22 are associated with increased susceptibility to optic nerve degeneration in glaucoma. PLoS Genet 8: e1002654.
15. Stoilova D, Child A, Trifan OC, Crick RP, Coakes RL, et al. (1996) Localization of a locus (GLC1B) for adult-onset primary open angle glaucoma to the 2cen-q13 region. Genomics 36: 142–150.
16. Akiyama M, Yatsu K, Ota M, Katsuyama Y, Kashiwagi K, et al. (2008) Microsatellite analysis of the GLC1B locus on chromosome 2 points to NCK2 as a new candidate gene for normal tension glaucoma. Br J Ophthalmol 92: 1293–1296.
17. Laakso M, Malkki M, Deeb SS (1995) Amino acid substitutions in hexokinase II among patients with NIDDM. Diabetes 44: 330–334.
18. Laakso M, Malkki M, Kekalainen P, Kuusisto J, Deeb SS (1995) Polymorphisms of the human hexokinase II gene: lack of association with NIDDM and insulin resistance. Diabetologia 38: 617–622.
19. Vidal-Puig A, Printz RL, Stratton IM, Granner DK, Moller DE (1995) Analysis of the hexokinase II gene in subjects with insulin resistance and NIDDM and detection of a Gln142–>His substitution. Diabetes 44: 340–346.
20. Echwald SM, Bjorbaek C, Hansen T, Clausen JO, Vestergaard H, et al. (1995) Identification of four amino acid substitutions in hexokinase II and studies of relationships to NIDDM, glucose effectiveness, and insulin sensitivity. Diabetes 44: 347–353.
21. da-Silva WS, Gomez-Puyou A, de Gomez-Puyou MT, Moreno-Sanchez R, De Felice FG, et al. (2004) Mitochondrial bound hexokinase activity as a preventive antioxidant defense: steady-state ADP formation as a regulatory mechanism of membrane potential and reactive oxygen species generation in mitochondria. J Biol Chem 279: 39846–39855.
22. Santiago AP, Chaves EA, Oliveira MF, Galina A (2008) Reactive oxygen species generation is modulated by mitochondrial kinases: correlation with mitochondrial antioxidant peroxidases in rat tissues. Biochimie 90: 1566–1577.
23. Majewski N, Nogueira V, Bhaskar P, Coy PE, Skeen JE, et al. (2004) Hexokinase-mitochondria interaction mediated by Akt is required to inhibit apoptosis in the presence or absence of Bax and Bak. Mol Cell 16: 819–830.
24. Inagaki Y, Mashima Y, Fuse N, Ohtake Y, Fujimaki T, et al. (2006) Mitochondrial DNA mutations with Leber's hereditary optic neuropathy in Japanese patients with open-angle glaucoma. Jpn J Ophthalmol 50: 128–134.
25. Buday L, Wunderlich L, Tamas P (2002) The Nck family of adapter proteins: regulators of actin cytoskeleton. Cell Signal 14: 723–731.
26. Suzuki S, Mizutani M, Suzuki K, Yamada M, Kojima M, et al. (2002) Brain-derived neurotrophic factor promotes interaction of the Nck2 adaptor protein with the TrkB tyrosine kinase receptor. Biochem Biophys Res Commun 294: 1087–1092.
27. Harada C, Guo X, Namekata K, Kimura A, Nakamura K, et al. (2011) Glia- and neuron-specific functions of TrkB signalling during retinal degeneration and regeneration. Nat Commun 2: 189.
28. Wu Y, Smas CM (2008) Expression and regulation of transcript for the novel transmembrane protein Tmem182 in the adipocyte and muscle lineage. BMC Res Notes 1: 85.
29. Nakano M, Ikeda Y, Taniguchi T, Yagi T, Fuwa M, et al. (2009) Three susceptible loci associated with primary open-angle glaucoma identified by genome-wide association study in a Japanese population. Proc Natl Acad Sci U S A 106: 12838–12842.
30. Anderson DR, VM P (1999) Automated Static Perimetry. 2nd edition. St.Louis: Mosby.
31. Funayama T, Ishikawa K, Ohtake Y, Tanino T, Kurosaka D, et al. (2004) Variants in optineurin gene and their association with tumor necrosis factor-alpha polymorphisms in Japanese patients with glaucoma. Invest Ophthalmol Vis Sci 45: 4359–4367.

Acknowledgments

The authors thank Dr. Duco I. Hamasaki for editing the manuscript, and thank Dr. Nariyuki Yamada and Prof. Makoto Tamai for experimental suggestions and support. We are grateful to Dr. Jun Kosaka for providing antibody mouse anti-C38.

Author Contributions

Conceived and designed the experiments: T. Funayama YM KN NF. Performed the experiments: DS T. Funayama YT AS KY MM AM TN NF. Analyzed the data: DS T. Funayama YM JER NF. Contributed reagents/materials/analysis tools: T. Funayama YT AS NY T. Fukuchi HA HI TN. Wrote the paper: DS KY JER NF.

Jpn J Ophthalmol (2013) 57:457–462
DOI 10.1007/s10384-013-0258-4

THE OFFICIAL INTERNATIONAL JOURNAL OF THE JAPANESE OPHTHALMOLOGICAL SOCIETY

CLINICAL INVESTIGATION

Development of a new strategy of visual field testing for macular dysfunction in patients with open angle glaucoma

Kazuko Omodaka · Shiho Kunimatsu-Sanuki · Ryu Morin · Satoru Tsuda · Yu Yokoyama · Hidetoshi Takahashi · Kazuichi Maruyama · Hiroshi Kunikata · Toru Nakazawa

Received: 19 January 2013 / Accepted: 27 May 2013 / Published online: 29 June 2013

Abstract
Purpose To explore methods of automated visual field (VF) examination for the assessment of macular function.
Method We used a VF examination (AP-7000 automatic perimeter, Kowa, Japan) to examine macular function in 53 eyes from 29 patients with open angle glaucoma. We measured the mean total deviation (c-MD) of 16 points in the central VF located in a 2-degree-interval 4 × 4 array with various stimulus sizes (Goldmann sizes III, II, and I). The retinal nerve fiber layer (RNFL) thickness, ganglion cell complex (GCC), and ganglion cell layer plus inner plexiform layer (GCL + IPL) were measured with the 3D OCT-2000 System (Topcon, Japan). The c-MDs of various stimulus sizes were compared with the OCT parameters using the Spearman rank correlation.
Results The average examination time was 93.5 ± 23.5 s and the c-MD values were −11.8 ± 8.2 (stimulus size III), −11.9 ± 9.5 (stimulus size II), and −12.3 ± 9.6 dB (stimulus size I). The c-MD (stimulus size III) and averaged total deviations of the Humphrey Field Analysis 10-2 program were significantly correlated ($\rho = 0.91$). The C-MD values for stimulus size III were significantly correlated with the OCT parameters (RNFL: $\rho = 0.59$; GCC: $\rho = 0.65$; and GCL + IPL: $\rho = 0.64$). The correlation coefficient between the c-MD and the GCC was better for stimulus sizes II and I ($\rho = 0.69$) than for stimulus size III ($\rho = 0.65$).
Conclusion The C-MD values for the 16 measured central VF points were significantly correlated with macular structure, and the smaller stimulus sizes of the automated VF test had a higher correlation coefficient of within 8°.

Keywords Macular function · Open angle glaucoma · Ganglion cell complex · Retinal nerve fiber layer

K. Omodaka · S. Kunimatsu-Sanuki · R. Morin · S. Tsuda · Y. Yokoyama · H. Takahashi · K. Maruyama · H. Kunikata · T. Nakazawa (✉)
Department of Ophthalmology, Tohoku University Graduate School of Medicine, 1-1 Seiryo-machi, Aoba-ku, Sendai, Miyagi 980-8574, Japan
e-mail: ntoru@oph.med.tohoku.ac.jp

Introduction

Glaucoma is characterized by glaucomatous optic neuropathy and a corresponding progressive degeneration of the retinal ganglion cells (RGCs). It is the second highest cause of blindness worldwide, affecting approximately 70 million people [1, 2]. One of the most significant risk factors for glaucoma progression is high intraocular pressure (IOP), and therapies to lower IOP have, therefore, become well established as treatments for primary open angle glaucoma (POAG) [3, 4]. Glaucoma progresses with age [5], and the increasing frequency of visual impairment is becoming a serious issue in Japan as the country's population ages.

In Asia, normal tension glaucoma (NTG) is more common than POAG [6–8], and IOP-lowering treatment is of more limited efficacy in this type of the disease. NTG eyes undergo significantly more damage nasally and inferiorly to the fixation point [9, 10]. Additionally, as we have previously demonstrated, the myopic disc type is significantly more common in patients with an advanced stage of NTG [11] and in patients with decreased visual acuity [12] when patients are classified by optic disc type [13, 14]. We found that these patients showed significant thinning of the temporal circumpapillary retinal nerve fiber layer thickness (cpRNFLT), including the papillomacular bundle. Decreased visual acuity in such patients may be related

to decreased tissue blood flow (filling defect) in the temporal optic disc [12]. Recently, patients with strong fluctuations in ocular perfusion pressure have been shown to have significant progression of visual field loss in the central 10° [15]. Decreased macular function is thus implicated in glaucoma, and decreased ocular perfusion pressure may be related to its pathogenesis.

Macular functions, including retinal sensitivity and visual acuity, are very important for quality of life even in patients with glaucoma [16]. Optical coherence tomography (OCT), which measures cpRNFLT, has proven, since its introduction by Huang et al. [17], to be useful in detecting and following the progression of glaucoma. Recently, spectral domain (SD) technology has led to a significant improvement in segmentation algorithms, and advances by several research groups have enabled us to visualize each retinal layer in the macular area, including the ganglion cell complex (GCC) and the ganglion cell layer plus inner plexiform layer (GCL + IPL) [18, 19]. Measurement of macular GCC thickness has the same performance in glaucoma diagnosis as cpRNFLT [20, 21], even in myopic patients [7]. Another tool used in glaucoma assessment is the Humphrey Field Analyzer (HFA). The 30-2 test pattern of the HFA has only 4 points within the central 4.2° (radius) of fixation, making the 10-2 test pattern a better choice to understand glaucomatous visual field damage in the central area of vision. However, using both test patterns on the same day can be fatiguing to patients because of the amount of time required. This means that, although glaucoma specialists can now use OCT to quickly and simply assess the structure of the macula, an equivalently quick and simple option to assess function is currently unavailable.

In this study, we sought to develop a method that allows evaluation of macular function with a shorter testing time and the results correlate well with those of both the 10-2 program of the HFA (HFA 10-2) and the OCT-measured retinal macular layer thickness. We evaluated parafoveal threshold testing (PTT), a new macular visual field examination with the AP-7000 automatic perimeter (Kowa Company, Nagoya, Japan). First, we investigated the correlation between the mean central total deviation (c-MD) at 16 test points, measured with PTT, and the average total deviation (TD) at 16 central test points, measured with the HFA 10-2. Second, we changed the stimulus size (Goldmann size III, II, or I) and compared the correlation of the measurement parameters taken from a macular OCT map (RNFL, GCC, and GCL + IPL) with the PTT c-MD values with different spot sizes. This method of measuring the macular visual field is quicker and less fatiguing for patients, enabling us to assess macular function more easily during the routine management of glaucoma patients.

Patients and methods

Inclusion criteria

This retrospective, cross-sectional study comprised 53 eyes of 29 Japanese adult patients with OAG. The cases were a continuous series, and all were introduced to the neuroprotective treatment unit of our department from March 2012 to September 2012. All the patients had visual field loss close to the fixation point, decreased visual acuity, and damage to the papillomacular bundle, and exhibited glaucomatous optic neuropathy. The inclusion criteria were: (1) diagnosis of OAG, including PAOG; (2) a spherical equivalent refractive error of >-8.00 D; and (3) a glaucomatous visual field meeting the Anderson-Patella classification. The exclusion criteria were: (1) decimal visual acuity <0.3 and (2) macular disease such as macular edema, macular degeneration, or premacular fibrosis.

The baseline clinical parameters recorded for each patient were age, sex, refractive error, and IOP. The baseline best-corrected visual acuity (BCVA) was measured with a standard Japanese decimal visual acuity chart and converted to the logarithm of the minimum angle of resolution (logMAR) for statistical analysis. IOP was measured with Goldmann applanation tonometry. Demographic data for the glaucoma patients of this study are listed in Table 1.

The study adhered to the tenets of the Declaration of Helsinki, and the protocols were approved by the Clinical Research Ethics Committee of Tohoku University Graduate School of Medicine.

AP-7000 automated perimeter

The AP-7000 is an instrument used to measure the visual field. It is functionally equivalent to the HFA. The hardware specifications for the AP-7000 for common static perimetry are the same as those for the HFA. The stimulus size is based on the Goldmann perimeter (sizes I to V). The examination distance is 300 mm. The maximum stimulus intensity is 10,000 asb. The stimulus presentation time is 0.2 s. The background intensity is 10 cd/m^2. Eye fixation is monitored with the Heijl–Krakau method. The AP-7000 has a fast-threshold strategy named "Quick." Basically, "Quick" is a staircase strategy with a single threshold crossing and a fixed step size of 3 dB. To more accurately detect abnormalities, a step size of 2 dB instead of 3 dB is adopted within a certain range of sensitivity based on a normative database.

Visual field analysis

Sixteen points in the central visual field were examined by means of PTT, all located in a 2°-interval 4 × 4 array (Fig. 1a, b). Various stimulus sizes (Goldmann sizes III, II,

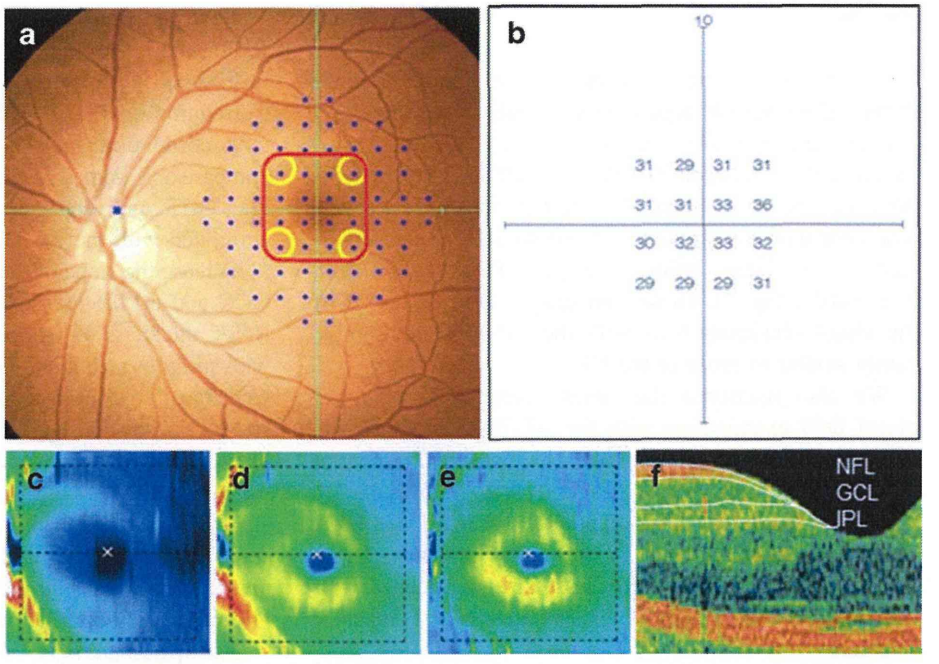

Fig. 1 Correspondence between parafoveal threshold testing (PTT) and the HFA 10-2. **a** Correspondence of the 16 PTT test points (red square) and the central 16 HFA 10-2 test points (68 blue dots). **b** Results from 16 PTT points. **c** Macular OCT map of the RNFL, **d** GCC, and **e** GCL + IPL from the 3D OCT-2000. OCT map with layer information. RNFL indicates nerve fiber layer; GCL, ganglion cell layer; and **f** IPL, inner plexiform layer

Table 1 Demographic data for the glaucoma patients of this study

	Mean ± standard deviation (range)
Male/female, eyes	30/23 (57 %/43 %)
Age, years	59.9 ± 12.9 (19–89)
Spherical equivalent, D	−3.1 ± 2.9 (−7.8 to 2.6)
Visual acuity, logMAR	0.10 ± 0.34 (−0.18 to 0.34)
MD of HFA 30-2, dB	−13.9 ± 8.4 (−29.4 to −0.3)
MD of HFA 10-2, dB	−18.8 ± 8.9 (−34.5 to −3.6)
Baseline IOP, mmHg	13.7 ± 2.7 (7–19)

MD mean deviation, *IOP* intraocular pressure

and I) were used and the c-MD values, measured. Standard automated perimetry was performed with the HFA. We used the Swedish interactive threshold algorithm (SITA)-standard strategy of the 10-2 program (Carl Zeiss Meditec, Dublin, CA, USA). The stimulus size of the HFA 10-2 was size III. HFA was performed within 3 months of the OCT measurement. Only reliable measurements of the visual field were included in the analysis (<20 % fixation errors, <33 % false-positive results, and <33 % false-negative results).

OCT macular map

The macular RNFL, GCC, and GCL + IPL thicknesses were measured using 3D OCT-2000 software (version 8.00; Topcon Corporation, Tokyo, Japan), with macular cube scans (a 6 × 6-mm square corresponding to a 20° square of the retina in the macular area) centered on the fovea. The thickness of each retinal layer was calculated automatically by the embedded 3D OCT software. Our analysis used the average thickness of the retinal layers in the area corresponding to the 16 central test points from the AP-7000 (an 8° square) (Fig. 1c–f). Although we found RGC and RNFL displacement in the fovea [22], the central 8° square was still suitable for analysis of the macula [22]. If the image quality score was <60, the image was excluded.

Correlation between structure and function in the parafovea

To analyze the right and left eyes together, all left eyes were flipped across the vertical midline to give the appearance of right eyes. We investigated the correlation of c-MDs measured with stimulus sizes III, II, and I with OCT-measured RNFL, GCC, and GCL + IPL, respectively.

Statistical analysis

The Spearman rank correlation was used to determine the correlations among the structural examination (RNFL, GCC, and GCL + IPL measured with the 3D OCT-2000), the results of the functional examination (c-MD and HFA 10-2 MD), and visual acuity. The significance level was set at $P < 0.05$. Statistical analysis was performed with JMP software (Pro version 9.0.2; SAS Institute Japan, Tokyo, Japan). A Z test was used to find the correlation coefficient level, with >1.96 set as the significance level.

Results

To determine whether the central 16 test points that we measured within a 8° square were valuable for clinical use in the management of glaucoma patients, we first compared the correlation between AP-7000 (c-MD) and average HFA 10-2 TDs in 16 corresponding test points. C-MD levels measured with a Goldmann size III stimulus were significantly correlated with average TDs ($\rho = 0.908$, $P < 0.0001$; Fig. 2). These data suggest that the results of the visual sensitivity tests with the AP-7000 are significantly similar to those of the HFA.

We also measured the times taken to complete a visual field examination with the AP-7000 and with the HFA 10-2. The mean time taken to measure the central 16 test points with the AP-7000 was 93.5 ± 23.5 s, while that with the SITA Standard test with the HFA 10-2 was 452.9 ± 63.5 s in the same patients. These data indicate that significantly less time was needed with the AP-7000 to complete an examination of macular function.

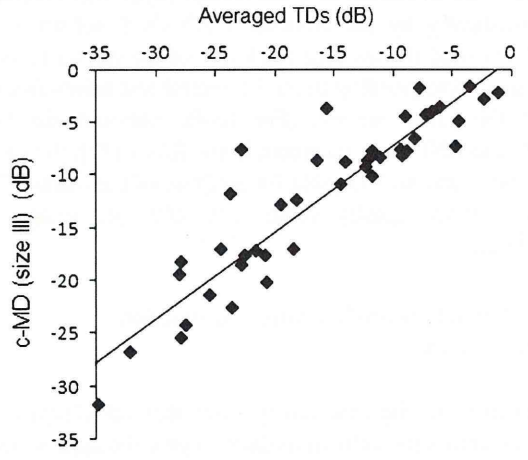

Fig. 2 Correlation between 16 PTT points and corresponding 16 HFA 10-2 points. Blot graph showing the correlation between 16-point PTT c-MD and average HFA 10-2 TD in the corresponding 16 test points. The formula of the correlation was $y = 0.82x + 0.92$, and the correlation coefficient was $\rho = 0.908$ ($P < 0.0001$)

Next, we compared c-MDs measured with stimulus sizes III, II, and I with the thicknesses of the RNFL, GCC, and GCL + IPL, respectively, from the OCT macular map. Correlation coefficients obtained from a single Spearman rank correlation analysis are listed in Table 2. All the comparisons were significantly correlated. From the macular OCT map data, the GCC thickness was the most correlated with the c-MD. A smaller stimulus size tended to increase the slope of the correlation formula between the GCC and c-MD, as shown in the blot graph (Fig. 3a–c). RNFL thickness was most correlated with results measured with stimulus size I, and GCC and GCL + IPL thicknesses were most correlated with results measured with stimulus size II. These data suggest that the power of the correlation between structure and function is different for each layer of the macula.

Finally, we compared macular function (c-MDs measured with stimulus size I, II, or III in the 16 central test points, as well as the entire area of the HFA 10-2) and visual acuity. Correlation coefficients obtained from a single Spearman rank correlation analysis are listed in Table 3. All the correlation coefficients were significant (Table 2). A Z test revealed that the only correlation coefficient showing a significant difference was between the entire area of the HFA 10-2 and the central area of the AP-7000, comprising the 16 central test points.

Discussion

In this study, we devised and tested a new strategy to evaluate macular function with the AP-7000 automated perimeter and found that it produced results comparable to those of the HFA. The average examination time for a central 4 × 4 set of test points was 93.5 ± 23.5 s. The C-MD results were significantly correlated with the average HFA 10-2 TD and the OCT-measured macular layer thickness. These data suggest that this new strategy can be used to quickly and accurately evaluate glaucoma patients with macular lesions.

The c-MD from the central 16 test points (within 8°) was significantly correlated with retinal layer thickness from

Table 2 Correlation coefficients for 16-point PTT and HFA 10-2

	PTT 16 pt			HFA 10-2
	III	II	I	Averaged TD (16 test points)
RNFL	$\rho = 0.591$*	$\rho = 0.636$*	$\rho = 0.638$*	$\rho = 0.589$*
GCC	$\rho = 0.651$*	$\rho = 0.693$*	$\rho = 0.691$*	$\rho = 0.672$*
GCL + IPL	$\rho = 0.642$*	$\rho = 0.684$*	$\rho = 0.677$*	$\rho = 0.659$*

PTT parafoveal threshold testing, *HFA* Humphrey Field Analyzer, *TD* total deviation, *RNFL* retinal nerve fiber layer, *GCC* ganglion cell complex, *GCL + IPL* ganglion cell layer plus inner plexiform layer

* $P < 0.0001$

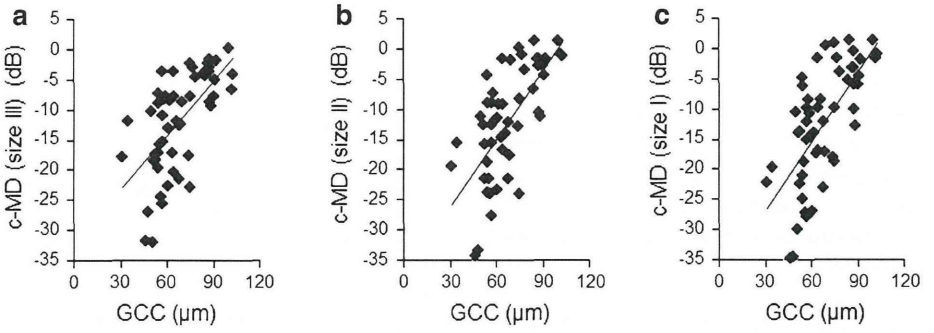

Fig. 3 Correlation between structure and function in the parafovea. *Blot graph* showing the correlation between GCC thickness and 16-point PTT c-MD with simulated stimulus sizes **a** III, **b** II, and **c** I. The formulas of correlation between GCC and the c-MD of stimulus sizes III, II, and I were $y = 0.30x - 32$ (III), $y = 0.38x - 38$ (II), and $y = 0.39x - 39$ (I), respectively

Table 3 Correlation coefficients between visual field and visual acuity

		Number of test points	ρ	*P* value
HFA 10-2	Central area	16	−0.421	<0.001
	Entire area	68	−0.302	0.019
PPT 16 pt	Size III	16	−0.474	<0.001
	Size II	16	−0.488	<0.001
	Size I	16	−0.463	<0.001

ρ correlation coefficient, *HFA* Humphrey Field Analyzer, *PTT* parafoveal threshold testing

the OCT macular map. The thicknesses of the macular RNFL [23], GCC [24], and GCL + IPL [22] were significantly correlated with macular function in glaucoma patients. This indicates that this new strategy using the AP-7000 can serve as a useful examination of macular function.

The value of this new system for central visual field testing is its speed and high correlation with the average HFA 10-2 TD and with OCT-measured macular layer thickness. Routine visual field tests often employ the 30-2 or 24-2 test of the HFA, but not the 10-2 test. The use of both on the same day is prohibitively time-consuming and fatiguing to the patient. Evaluation of the macula with OCT has many benefits, including its objective and quantitative nature and its less-burdensome examination procedure. However, OCT is a simple anatomical measurement of the retinal layer's thickness, and is, therefore, not a perfect alterative to a functional examination of the macula. Additionally, there is presently no useful electrophysiological examination of macular RGCs. Therefore, our new strategy is worthwhile in many situations arising in the management and follow-up of glaucoma patients.

The correlation of stimulus size with macular OCT parameters differed for Goldmann stimulus sizes I, II, and III. The correlation coefficient between macular structure and function for stimulus sizes I and II was larger than that for stimulus size III. For the central examination points of the HFA 30-2, a stimulus size of III covers an area of the retina containing approximately 150 RGCs. This makes the density of RGCs significantly higher than it would be in the peripheral retina [25]. The area that the Goldmann spots stimulate increases 4-fold with each step (size I: 0.25 mm^2; size II: 1 mm^2; size III: 4 mm^2), and, theoretically, smaller stimulus sizes should stimulate a smaller number of RGCs. In addition, we found that the correlation coefficient for stimulus size I was highest for the RNFL, but for stimulus size II, it was higher for the GCC and the GCL + IPL. Because of the macula's anatomy [26], the fovea has no RGCs or RNFL. We found that the anatomical displacement of the RNFL was more pronounced in the parafoveal area than in the GCC or GCL + IPL, which may have affected the correlation coefficient. It is hard to judge the best stimulus size for the macular area by considering only the higher correlation coefficient for the smaller stimulus size. It is also necessary to consider the effect of the stimulus size on the dynamic range of visual sensitivity, the fluctuation range of the threshold, and the opacity of the optic media.

This study had several limitations. First, it involved only a small number of glaucoma patients. Second, factors such as age, axonal length, glaucoma stage, and myopia were reported to be associated with bias in the correlation between structure and function [27, 28]. To decrease the influence of these factors on the results, we excluded glaucoma patients with high myopia (less than −8 D). Third, since this study was retrospective, macular assessment in the glaucoma patients had an inbuilt selection bias because macular lesions are not always involved in the disease process of glaucoma. Fourth, glaucoma patients with focal damage outside the examination area (the 16 central test points of the AP-7000) were outside the scope of this evaluation method.

In conclusion, we found that an examination of only the 16 central points of the HFA 10-2 test shortened testing time and correlated well with both the average HFA 10-2 TD (16 central test points) and the OCT-measured retinal macular layer thickness. A small stimulus size also helped improve the sensitivity of the evaluation of macular function. This macular sectorial approach can likely improve the accuracy of examinations of glaucoma patients with decreased macular function.

Acknowledgments The authors thank Mr Yukihiro Shiga and Mr Ryou Watanabe for data acquisition, and Mr Tim Hilts for editing of this manuscript.

References

1. Quigley HA. Number of people with glaucoma worldwide. Br J Ophthalmol. 1996;80:389–93.
2. Quigley HA, Dunkelberger GR, Green WR. Retinal ganglion cell atrophy correlated with automated perimetry in human eyes with glaucoma. Am J Ophthalmol. 1989;107:453–64.
3. Heijl A, Leske MC, Bengtsson B, Hyman L, Hussein M. Reduction of intraocular pressure and glaucoma progression: results from the Early Manifest Glaucoma Trial. Arch Ophthalmol. 2002;120:1268–79.
4. Kass MA, Heuer DK, Higginbotham EJ, Johnson CA, Keltner JL, Miller JP, et al. The Ocular Hypertension Treatment Study: a randomized trial determines that topical ocular hypotensive medication delays or prevents the onset of primary open-angle glaucoma. Arch Ophthalmol. 2002;120:701–13 (discussion 829–30).
5. Quigley HA, Broman AT. The number of people with glaucoma worldwide in 2010 and 2020. Br J Ophthalmol. 2006;90:262–7.
6. Iwase A, Suzuki Y, Araie M, Yamamoto T, Abe H, Shirato S, et al. The prevalence of primary open-angle glaucoma in Japanese: the Tajimi Study. Ophthalmology. 2004;111:1641–8.
7. Kim CS, Seong GJ, Lee NH, Song KC. Prevalence of primary open-angle glaucoma in central South Korea: the Namil study. Ophthalmology. 2011;118:1024–30.
8. Liang YB, Friedman DS, Zhou Q, Yang X, Sun LP, Guo LX, et al. Prevalence of primary open angle glaucoma in a rural adult Chinese population: the Handan eye study. Invest Ophthalmol Vis Sci. 2011;52:8250–7.
9. Araie M, Arai M, Koseki N, Suzuki Y. Influence of myopic refraction on visual field defects in normal tension and primary open angle glaucoma. Jpn J Ophthalmol. 1995;39:60–4.
10. Mayama C, Suzuki Y, Araie M, Ishida K, Akira T, Yamamoto T, et al. Myopia and advanced-stage open-angle glaucoma. Ophthalmology. 2002;109:2072–7.
11. Nakazawa T, Fuse N, Omodaka K, Aizawa N, Kuwahara S, Nishida K. Different types of optic disc shape in patients with advanced open-angle glaucoma. Jpn J Ophthalmol. 2010;54:291–5.
12. Omodaka K, Nakazawa T, Yokoyama Y, Doi H, Fuse N, Nishida K. Correlation between peripapillary macular fiber layer thickness and visual acuity in patients with open-angle glaucoma. Clin Ophthalmol. 2010;4:629–35.
13. Nicolela MT, Drance SM. Various glaucomatous optic nerve appearances: clinical correlations. Ophthalmology. 1996;103:640–9.
14. Nicolela MT, McCormick TA, Drance SM, Ferrier SN, LeBlanc RP, Chauhan BC. Visual field and optic disc progression in patients with different types of optic disc damage: a longitudinal prospective study. Ophthalmology. 2003;110:2178–84.
15. Sung KR, Cho JW, Lee S, Yun SC, Choi J, Na JH, et al. Characteristics of visual field progression in medically treated normal-tension glaucoma patients with unstable ocular perfusion pressure. Invest Ophthalmol Vis Sci. 2011;52:737–43.
16. Sumi I, Shirato S, Matsumoto S, Araie M. The relationship between visual disability and visual field in patients with glaucoma. Ophthalmology. 2003;110:332–9.
17. Huang D, Swanson EA, Lin CP, Schuman JS, Stinson WG, Chang W, et al. Optical coherence tomography. Science. 1991;254:1178–81.
18. Mwanza JC, Oakley JD, Budenz DL, Chang RT, Knight OJ, Feuer WJ. Macular ganglion cell-inner plexiform layer: automated detection and thickness reproducibility with spectral domain-optical coherence tomography in glaucoma. Invest Ophthalmol Vis Sci. 2011;52:8323–9.
19. Morooka S, Hangai M, Nukada M, Nakano N, Takayama K, Kimura Y, et al. Wide 3-dimensional macular ganglion cell complex imaging with spectral-domain optical coherence tomography in glaucoma. Invest Ophthalmol Vis Sci. 2012;53:4805–12.
20. Kim NR, Lee ES, Seong GJ, Kim JH, An HG, Kim CY. Structure-function relationship and diagnostic value of macular ganglion cell complex measurement using Fourier-domain OCT in glaucoma. Invest Ophthalmol Vis Sci. 2010;51:4646–51.
21. Seong M, Sung KR, Choi EH, Kang SY, Cho JW, Um TW, et al. Macular and peripapillary retinal nerve fiber layer measurements by spectral domain optical coherence tomography in normal-tension glaucoma. Invest Ophthalmol Vis Sci. 2010;51:1446–52.
22. Raza AS, Cho J, de Moraes CG, Wang M, Zhang X, Kardon RH, et al. Retinal ganglion cell layer thickness and local visual field sensitivity in glaucoma. Arch Ophthalmol. 2011;129:1529–36.
23. Sakamoto A, Hangai M, Nukada M, Nakanishi H, Mori S, Kotera Y, et al. Three-dimensional imaging of the macular retinal nerve fiber layer in glaucoma with spectral-domain optical coherence tomography. Invest Ophthalmol Vis Sci. 2010;51:5062–70.
24. Na JH, Kook MS, Lee Y, Baek S. Structure-function relationship of the macular visual field sensitivity and the ganglion cell complex thickness in glaucoma. Invest Ophthalmol Vis Sci. 2012;53:5044–51.
25. Kerrigan-Baumrind LA, Quigley HA, Pease ME, Kerrigan DF, Mitchell RS. Number of ganglion cells in glaucoma eyes compared with threshold visual field tests in the same persons. Invest Ophthalmol Vis Sci. 2000;41:741–8.
26. Drasdo N, Millican CL, Katholi CR, Curcio CA. The length of Henle fibers in the human retina and a model of ganglion receptive field density in the visual field. Vis Res. 2007;47:2901–11.
27. Kang SH, Hong SW, Im SK, Lee SH, Ahn MD. Effect of myopia on the thickness of the retinal nerve fiber layer measured by Cirrus HD optical coherence tomography. Invest Ophthalmol Vis Sci. 2010;51:4075–83.
28. Leung CK, Yu M, Weinreb RN, Ye C, Liu S, Lai G, et al. Retinal nerve fiber layer imaging with spectral-domain optical coherence tomography: a prospective analysis of age-related loss. Ophthalmology. 2012;119:731–7.

Journal of Neurochemistry

JOURNAL OF NEUROCHEMISTRY | 2013 | 127 | 669–680 doi: 10.1111/jnc.12325

ORIGINAL ARTICLE

Critical role of Nrf2 in oxidative stress-induced retinal ganglion cell death

Noriko Himori,* Kotaro Yamamoto,* Kazuichi Maruyama,* Morin Ryu,* Keiko Taguchi,† Masayuki Yamamoto† and Toru Nakazawa*

*Department of Ophthalmology, Tohoku University Graduate School of Medicine, Sendai, Miyagi, Japan

†Department of Medical Biochemistry, Tohoku University Graduate School of Medicine, Sendai, Miyagi, Japan

Abstract

NF-E2 related factor 2 (Nrf2) is a key transcription factor that plays a pivotal role in endogenous protection against oxidative stress. However, the role of Nrf2 in visual disorders remains unclear. It has been reported that oxidative stress is thought of as one of the causes of glaucoma. Here, we investigate whether the function of Nrf2 in oxidative stress-induced retinal ganglion cell (RGC) death. This study used adult male Nrf2 deficient mice (Nrf2 KO) and age- and sex-matched wild-type (WT) mice. We dissociated and purified *N*-4-[4-didecylaminostryryl]-*N*-methyl-pyridinium iodide-labeled RGCs with fluorescence-activated cell sorting, and tried to detect the *Nrf2* and *Keap1* genes. In the absence of nerve crush (NC), the number of RGCs in Nrf2 KO mice was almost same as that in WT mice. 1-(2-cyano-3-, 12-dioxooleana-1, 9 (11)-dien-28-oyl) imidazole (CDDO-Im), an Nrf2 activator, prevented NC-induced loss of RGCs in WT mice. Seven days after NC, without treatment, the number of RGCs in Nrf2 KO mice was significantly lower than in WT mice. In addition, after CDDO-Im treatment, quantitative RT-PCR showed increased expression of antioxidant and phase II detoxifying enzymes. These results suggest that up-regulation of Nrf2 signaling after CDDO-Im treatment may be a novel therapeutic strategy for the protection of RGCs, especially in glaucoma.

Keywords: glaucoma, neuroprotection, Nrf2, oxidative stress, retinal ganglion cell.

J. Neurochem. (2013) **127**, 669–680.

Glaucoma is well known to be one of the world's major causes of secondary blindness (Quigley 1996). It is thought that the ultimate cause of vision loss in this disease is retinal ganglion cell (RGC) apoptosis (Yücel *et al.* 2003). Therefore, the neuroprotection of RGCs has recently drawn attention as a new approach to glaucoma therapy.

Several hypotheses have been proposed for potential mechanisms triggering RGC death in glaucoma, including compromised blood flow at the optic nerve (Hayreh 1997; Kerr *et al.* 1998), nitric oxide–induced injury to the optic nerve (Neufeld *et al.* 1999; Shareef *et al.* 1999; Liu and Neufeld 2001), and glutamate excitotoxicity (Vorwerk *et al.* 1999; Sullivan *et al.* 2006; Seki and Lipton 2008). In addition to these primary mechanisms, some studies have provided evidence that oxidative stress contributes to the degeneration of RGCs in glaucoma (Izzotti *et al.* 2006; Engin *et al.* 2010; Ferreira *et al.* 2010; Bagnis *et al.* 2012). However, the precise nature of RGC damage caused by oxidative stress remains unclear.

NF-E2-related factor2 (Nrf2) is a transcription factor that is activated by oxidative stress and the presence of electrophiles, controlling hundreds of detoxifying and antioxidant

Received April 22, 2013; revised manuscript received May 28, 2013; accepted May 29, 2013.

Address correspondence and reprint requests to Toru Nakazawa, Department of Ophthalmology, Tohoku University Graduate School of Medicine, 1-1 Seiryo, Aoba, Sendai, Miyagi, 980-8574, Japan.
E-mail: ntoru@oph.med.tohoku.ac.jp

Abbreviations used: 4Di-10ASP, *N*-4-[4-didecylaminostryryl]-*N*-methyl-pyridinium iodide; ARE, antioxidant response elements; CDDO-Im, 1-(2-cyano-3-, 12-dioxooleana-1, 9 (11)-dien-28-oyl) imidazole; DAB, diaminobenzidine; FACS, fluorescence-activated cell sorting; FG, fluorogold; GCL, ganglion cell layer; HBSS, Hank's buffered saline solution; HNE, hydroxynonenal; IOP, intraocular pressure; Keap1, Kelch-like ECH associated protein 1; NC, nerve crush; Nrf2 KO, Nrf2 deficient mice; Nrf2, NF-E2 related factor 2; NTG, normal tension glaucoma; OAG, open angle glaucoma; OHdG, hydroxy-2′-deoxyguanosine; PVDF, polyvinylidene fluoride; QPCR, quantitative RT-PCR; RGC, retinal ganglion cell; ROS, reactive oxygen species; RT-PCR, reverse transcription PCR; TBARS, thiobarbituric acid reactive substances; WT, wild type.

genes. Under basal conditions, the cytosolic regulatory protein Kelch-like ECH associated protein 1 (Keap1) sequesters Nrf2 in the cytoplasm. Upon exposure to oxidative or electrophilic stress, Nrf2 is released from Keap1 repression and translocates to the nucleus where it heterodimerizes with small Maf proteins to enhance transcription of the target genes via antioxidant response elements in the promoters (Itoh *et al.* 1997). In Nrf2 knockout (Nrf2 KO) mice, induction of antioxidant response elements-dependent cytoprotective genes is severely impaired, making them susceptible to a variety of pharmacological and environmental toxicants (Aoki *et al.* 2001; Enomoto *et al.* 2001; Osburn and Kensler 2008; Uno *et al.* 2010). This makes Nrf2 KO mice useful to investigate the role of oxidative stress in the pathological condition of eye diseases (Nagai *et al.* 2009; Zhao *et al.* 2011; Shanab *et al.* 2012).

Normal tension glaucoma (NTG), in which patients have normal intraocular pressure, is an important subset of open angle glaucoma. NTG is also more prevalent in the Asian population (Iwase *et al.* 2004). Interestingly, both glutamate excitotoxicity and oxidative stress are involved in RGC death in glutamate transporter KO mice, a model of NTG (Harada *et al.* 2007). Our present data was derived from experiments based on nerve crush (NC), which is a commonly used model of axonal injury. It provides insight into the mechanisms involved in the death of the RGCs by providing a precise, short-term synchronous insult to the axons. This results in secondary RGC apoptotic cell death that resembles glaucoma. Therefore, NC should be a good model for the investigation of NTG.

Nrf2 has shown strong potential to protect against a broad range of diseases associated with oxidative stress (Clements *et al.* 2006; Padmanabhan *et al.* 2006; Satoh *et al.* 2006; Singh *et al.* 2006). However, its role in the glaucoma model remains unclear. In this study, we hypothesize that Nrf2 protects retinal neurons from oxidative stress. To elucidate this role, we investigated the functions of Nrf2 in NC-induced RGC death. We also tested whether enhancing Nrf2 signaling with the extremely potent synthetic triterpenoid activator 1-(2-cyano-3,12-dioxooleana-1,9(11)-dien-28-pyl)imidazole (CDDO-Im) (Liby *et al.* 2005), protects against oxidative stress-induced RGC death. In short, we explored whether CDDO-Im had a neuroprotective effect against RGC damage.

Method

Animals

Male Nrf2 KO mice (C57BL/6J mouse background, 10–12 weeks old, 20–25 g: The Nrf2 KO mice were bred and maintained at our institution, and were kindly provided by Dr. Masayuki Yamamoto and Dr. Keiko Taguchi) and age- and sex-matched C57BL/6J mice were housed in covered cages. The mice were genotyped for Nrf2 status with PCR amplification of genomic DNA extracted from tail snips (Aoki *et al.* 2007). PCR amplification was performed using three different primers: 5′-TGGACGGGACTATTGAAGGCTG-3′ (sense for both genotypes), 5′-GCCGCCTTTTCAGTAGATGGA GG-3′ (antisense for wild type), and 5′-GCGGATTGACCGTAA TGGGATAGG-3′ (antisense for LacZ). All animals were maintained and handled in accordance with the guidelines of the Association for Research in Vision and Ophthalmology Statement for the Use of Animals in Ophthalmic and Vision Research and the guidelines from the declaration of Helsinki and the Guiding Principles in the Care and Use of Animals. All experimental procedures described in this study were approved by the Ethics Committee for Animal Experiments at Tohoku University Graduate School of Medicine, and were performed according to the National Institutes of Health guidelines for the care and use of laboratory animals.

Immunohistochemistry

The eyes were enucleated and washed, then fixed in 4% paraformaldehyde overnight at 4°C, immersed in a 20% sucrose solution, and embedded in an optimal cutting temperature compound (Sakura Finetechnical Co. Ltd., Tokyo, Japan). Transverse 10 μm-thick cryostat sections were cut and placed onto slides (MAS COAT; Matsunami Glass Ind. Ltd., Osaka, Japan). Immunohistochemical staining has been described previously (Inokuchi *et al.* 2009). Briefly, the tissue sections were washed in 0.01 M phosphate-buffered saline (PBS) for 10 min. We used 8-hydroxy-2′-deoxyguanosine (OHdG) and 4-hydroxynonenal (HNE) mouse monoclonal antibody (Japan Institute for the Control of Aging, Shizuoka, Japan). When 8-OHdG was used, the primary antibody was incubated at 4°C overnight. With 4-HNE, the tissue sections were incubated with the antibody for 1 h. Next, endogenous peroxidase was quenched by treating the sections with 3% hydrogen peroxide in absolute methanol for 10 min. The sections were washed, and then incubated with biotinylated anti-mouse IgG. They were subsequently incubated with the avidin-biotin-peroxidase complex for 30 min, and were then developed using diaminobenzidine peroxidase substrate for 1 min.

Thiobarbituric acid reactive substances

The levels of thiobarbituric acid reactive substances (TBARS) in the retinas were analyzed (Ferreira *et al.* 2010; Salido *et al.* 2012). Each retina was homogenized in 56 mM potassium chloride buffer and centrifuged at 20 000 g for 10 min at 4°C. The sediment was used for analysis. It was mixed with 8.1% sodium dodecyl sulfate, 0.8% 2-Thiobarbituric acid and 20% acetic acid. The samples were heated for 1 h at 100°C. After they had cooled, they were measured with fluorescence at an excitation wavelength of 530 nm and an emission wavelength of 550 nm with a Kinetic Microplate Reader (Molecular Devices, Sunnyvale, CA, USA). The results were normalized to protein concentration.

Oxidative stress and mitochondrial proteins

Retrograde labeling was performed as described below. Seven days afterwards, optic nerve surgery was performed, and after seven more days, the retinas were harvested. The retinas were then washed with Dulbecco's phosphate-buffered saline and stained with both 500 nM MitoTracker Deep Red FM (Invitrogen, Carlsbad, CA, USA) and 5 μM CellRox Green Reagent (Invitrogen) at 4°C for 2 h. After washes with Dulbecco's phosphate-buffered saline, the retinas were fixed with 4% paraformaldehyde at 4°C for 2 h, and were then flat mounted onto glass slides. Imaging was performed with a confocal

laser-scanning microscope (LSM5 PASCAL; Carl Zeiss, Jena, Germany).

Retrograde labeling and counting of RGC

Retrograde labeling was performed as described in our previous research (Nakazawa *et al.* 2007b; Ryu *et al.* 2012). Briefly, RGCs were retrogradely labeled with a fluorescent tracer, Fluoro-gold (FG; Fluorochrome, LLC, Denver, CO, USA), or carbocyanine dye, *N*-4-[4-didecylaminostryryl]-*N*-methyl-pyridinium iodide (4Di-10ASP; Molecular Probes, Eugene, OR, USA). 1 μL of 2% aqueous FG in 1% dimethylsulfoxide or of 3% 4Di-10ASP in dimethylformamide was injected into the superior colliculus with a 32 G needle.

Seven days after FG labeling, a NC procedure was performed in the right eye only. Seven days after NC, the mice were killed and their complete retinas were placed on glass slides with the ganglion cell layer facing up. Vectashield mounting medium (Vector Laboratories, Burlingame, CA, USA) and cover glass were applied. RGC density was determined by counting tracer-labeled RGCs in 12 distinct areas under the microscope, as previously described (Nakazawa *et al.* 2002a,b).

RGC purification

Seven days after retrograde labeling, the 4Di-10ASP-labeled mice were killed. The retinas were rapidly dissected, incubated in a digestion solution containing papain (10 U/mL; Worthington-Biochemical Co., Lakewood, NJ, USA) and L-cysteine (0.3 mg/mL; Sigma-Aldrich, St Louis, MO, USA) in Hank's Buffered Saline Solution (Invitrogen), and incubated at 37°C for 15 min (CO_2 incubator). The retinas were rinsed twice in Hank's Buffered Saline Solution, and dissociated in Neurobasal A medium containing a B27 supplement (NBA/B27 AO+; Invitrogen). The dissociated cells were passed through a cell strainer (40 μm nylon net; BD-Falcon, Bedford, MA, USA), cooled to 4°C, and immediately sorted using a fluorescence-activated cell sorting (FACS) Aria II (Becton-Dickinson, San Jose, CA, USA). A 585/42 filter was used to detect the 4Di-10ASP-labeled RGCs. The cells were sorted directly into 350 μL of buffer RLT Plus (RNeasy kit; Qiagen, Valencia, CA, USA) with 1% β-mercaptoethanol, frozen immediately, and stored at −80°C until further use. The sorted cells were placed in serum-free media without growth factors, and the yield, purity, and viability of the RGCs were determined after 2 h in culture. To determine the immunocytochemistry of the RGC marker Thy1, retinal cells were incubated, on ice, with FITC-conjugated anti-Thy1 antibody (12.5 μg/mL; BD Biosciences, San Diego, CA, USA) for 30 min. They were then treated with isotype-matched nonspecific IgG antibodies, which were used as isotype controls. Finally, the sorted RGCs were re-suspended in medium and observed with a microscope. Independent sets of samples were prepared, each containing 6000 RGCs, for each experimental condition, namely, RGCs subjected to NC injury and normal controls. Total RNA was extracted from FACS-purified RGCs using RNeasy Micro Kit (Qiagen), according to the manufacturer's protocol. The RNA was then concentrated using RNeasy MinElute Spin columns (Qiagen).

Immunoblot analysis

One day after nerve crush, the retinas were rinsed in PBS for protein expression analysis. Nuclear extract was isolated using NE-PER Nuclear and Cytoplasmic Extraction Reagents (Thermo Scientific, Rockford, IL, USA) according to the manufacturer's instructions. The nuclear and cytoplasmic fractions were first treated with SDS sample buffer, and then heated to 100°C, for 5 min. Protein concentrations were measured using the bicinchoninic acid protein assay kit (Thermo Scientific). Each sample was separated with sodium dodecyl sulfate–polyacrylamide gel electrophoresis and electroblotted onto a polyvinylidene fluoride membrane (Millipore, Bedford, MA, USA). After non-specific binding had been blocked with 4% BlockAce (Yukijirushi, Sapporo, Japan), the membranes were incubated at 4°C overnight with a rabbit monoclonal antibody against Nrf2 (1 : 500; Cell signaling Technology, Beverly, MA, USA), β-actin (1 : 1000; Sigma-Aldrich) and TATA binding protein (1 : 500; Cell signaling Technology). The membranes were then incubated with a horseradish peroxidase-conjugated rabbit immunoglobulin secondary antibody for 1 h. The signals were visualized with chemiluminescence (ECL blotting Analysis System; Amersham, Arlington Heights, IL, USA) and measured in Image Lab statistical software (Bio-Rad, Hercules, CA, USA). Cytoplasmic fractions were normalized to β–actin and nuclear fractions were normalized to TATA binding protein.

Reverse transcription PCR with retinas from Nrf2 KO mice

Total RNA extraction and RT-PCR were performed as previously reported, with minor modifications (Nakazawa *et al.* 2006a). RT-PCR was performed with RNA from the retinas of Nrf2 KO and wild-type (WT) mice. The RT-PCR thermocycle program (PCR Thermal Cycler MP; Takara Bio, Shiga, Japan) consisted of denaturation at 94°C for 4 min, followed by 27 cycles of denaturation at 94°C for 30 s, annealing at 61°C for 30 s, and an extension at 72°C for 30 s. The final extension was at 72°C for 10 min. The primer sets used in this study were as follows (*Nrf2*: F: TGCCCCTCATCAGGCCCAGT; R: GCTCGGCTGGGACTCG TGTT, *Keap1*: F: GGTGGCGCGCTGTGCTTAGT; R: TGCTG GCTCAGGCGAAGCTC, and *Gapdh*: F: TCTGACGTGCCGCCT GGAGA; R: GGGGTGGGTGGTCCAGGGTT). The expected product length was 588 bp (*Nrf2*), 340 bp (*Keap1*), and 299 bp (*Gapdh*).

Quantitative RT-PCR

Quantitative RT-PCR (QPCR) was performed as previously described (Nakazawa *et al.* 2006b, 2007a,b) with minor modifications. The retinas were sampled and immediately sunk in RNA stabilization reagent (RNase later sample and assay technology; Qiagen). Total RNA was extracted from the retinas and purified RGCs (6000 RGCs) as described above with the RNeasy Micro Kit (Qiagen) and cDNA was synthesized with SuperScript III reverse transcriptase (Invitrogen). QPCR was performed with a 7500 Fast Real Time PCR System (Applied Biosystems, Foster city, CA, USA) by TaqMan Gene Expression Assays (Applied Biosystems). TaqMan Fast Universal PCR master mix (Applied Biosystems) was used for QPCR to quantify mRNA levels with commercially available TaqMan probes for *Thy1* (Mm00493682_g1), *Nrf2* (Mm00477786_m1), *Keap1* (Mm00497268_m1), *Nqo1* (Mm00500821_m1), *Ho-1* (Mm00516007_m1), *Gsta4* (Mm00494803_m1), *Txnrd* (Mm00443675_m1), *Gclm* (Mm00514997_m1), *Gclc* (Mm00802657_g1), and *Gapdh* (Mm99999915_g1). The mRNA levels were normalized to *Gapdh* as an internal control.